Arsenate Incorporation in Gypsum Probed by Neutron, X-ray Scattering and Density Functional Theory Modeling

Alejandro Fernández-Martínez,* Gabriel J. Cuello, Mark R. Johnson, Fabrizio Bardelli, Gabriela Román-Ross, Laurent Charlet, and Xavier Turrillas

LGIT, University of Grenoble and CNRS, B.P. 53, 38041 Grenoble Cedex 9, France, Institut Laue-Langevin, B.P. 156, 38042 Grenoble Cedex 9, France, Departament of Chemistry, University of Girona, Campus de Montilivi, 17071 Girona, Spain, INFM-GILDA c/o ESRF, B.P. 220, 38043 Grenoble Cedex 9, France, and Eduardo Torroja Institute for Construction Sciences, Spanish Council of Scientific Research, Serrano Galvache 4, 28033 Madrid, Spain

Received: July 31, 2007; Revised Manuscript Received: March 24, 2008

The ability of gypsum, a common sulfate mineral, to host arsenic atoms in its crystalline structure, is demonstrated through experimental structural studies of the solid solutions formed upon synthetic coprecipitation of gypsum ($CaSO_4 \cdot 2H_2O$) and arsenic. Neutron and X-ray diffraction methods show an enlargement of the gypsum unit cell proportional to the concentration of arsenic in the solids and to the pH solution value. The substitution of sulfate ions (SO_4^{2-}) by arsenate ions is shown to be more likely under alkaline conditions, where the $HAsO_4^{2-}$ species predominates. A theoretical Density Functional Theory model of the arsenic-doped gypsum structure reproduces the experimental volume expansion. Extended X-ray Absorption Fine Structure (EXAFS) measurements of the local structure around the arsenic atom in the coprecipitated solids confirm solid state substitution and allow some refinement of the local structure, corroborating the theoretical structure found in the simulations. The charge redistribution within the structure upon substitutions of either the protonated or the unprotonated arsenate species studied by means of Mulliken Population Analyses demonstrates an increase in the covalency in the interaction between Ca^{2+} and AsO_4^{3-}, whereas the interaction between Ca^{2+} and $HAsO_4^{2-}$ remains predominantly ionic.

1. Introduction

Arsenic is a metalloid widely distributed in the biosphere and highly toxic.[1,2] It is present in many industrial sites where mineral ores of lead, copper, zinc, tin, cobalt, gold or silver have been smelted.[3] Some As-bearing minerals (like Arsenopyrite FeAsS) are used as raw materials for some of these processes, causing the release of high quantities of arsenic to the environment in the form of arsenite (As^{3+}) or arsenate (As^{5+}).[4,5] The toxicity of arsenic depends on its physicochemical forms, the arsenite species being more mobile and toxic than arsenate. Redox transformations also play an important role in the arsenic availability to the environment. Changes in the redox state can give rise to precipitation processes of solid phases, thus decreasing the concentration of arsenic in groundwaters.[5–7] The solubility of these solid phases controls the concentration of arsenic aqueous species that are available to the environment. Coprecipitation of As-free minerals like gypsum in the presence of arsenic may lead to long-term immobilization of the contaminant, until the host phase is dissolved. For this reason a good understanding of the interactions between the solid and the contaminant and the underlying substitution process is required.

The study of ion substitution in minerals has a big impact in the study of the long-term retention of contaminants (as As,[6,8–10] Hg,[11] lanthanides,[12] or actinides[13,14]) in polluted environments or potential contaminated sites, as nuclear waste repositories.[15] Substitution processes of arsenic on the calcite surface[16] and into its bulk[8–10] have been recently reported. Substitutions of divalent cations such as Co^{2+}, Zn^{2+}, Mn^{2+}, Ni^{2+} or UO_2^{2+} and trivalent cations such as Cm^{3+} or Am^{3+} in calcite have been largely studied by bulk sensitive techniques as X-ray absorption spectroscopy (XAS), X-ray standing waves, electron paramagnetic resonance (EPR), neutron diffraction and time resolved laser fluorescence spectroscopy methods.[13,14,17–22]

Gypsum is a common industrial byproduct from a number of processes involving neutralization of sulfuric acid and SO_2-rich fumes.[23,24] Some industrial activities where mineral ores are smelted generate As-rich gypsum sludges, produced upon neutralization of As-rich acidic solutions. Quite often, gypsum from those sludges appears associated with Ca arsenates.[4] However, little is known about arsenic incorporation into the bulk of gypsum, which may potentially lead to its long-term immobilization into the mineral structure.

Incorporation of anions into the structure of sulfate minerals has been little studied. Paktunc and Dutrizac have demonstrated the ability of jarosite, a sulfate mineral, to host arsenate anions by substitution for sulfate.[25] Fernández-González et al. have studied the incorporation of selenate anions SeO_4^{2-} into the sulfate site of gypsum, revealing the complete miscibility diagram for sulfate/selenate substitutions.[26] The arsenate ion, with C_2 tetrahedral symmetry, has a very similar geometry to sulfate, with T_d symmetry, thus opening the hypothesis of an arsenate for sulfate substitution in the bulk of gypsum.

In this paper we present the results of a crystallographic study of synthetic gypsum coprecipitated with arsenic at different concentrations and pH values. Solid phases have been studied by neutron and X-ray diffraction experiments. X-ray absorption spectroscopy experiments reveal the local structure of the arsenate ions within the gypsum crystallographic structure.

* Corresponding author. Tel: +33 (0)4 76 20 75 71. Fax: +33 (0)4 76 20 76 48. E-mail: fernande@ill.fr.

10.1021/jp076067r CCC: $40.75
Published on Web 05/20/2008

TABLE 1: Description of the Samples with the Initial Concentration of As(V) in Solution and Total Concentration of As(V) in the Solids (Adsorbed and Substituted) As Measured by ICP-AES[a]

sample label	pH	predominant As species	initial [As(V)] in solution (M)	[As(V)] in solids (mM/kg)
Y0	7.5	~50% $H_2AsO_4^-$ ~50% $HAsO_4^{2-}$	0	0
Y1	4	$H_2AsO_4^-$	0.01	
Y2	4		0.04	121
Y3	4		0.06	60.28
Y4	4		0.09	371
Y5	7.5	~50% $H_2AsO_4^-$ ~50% $HAsO_4^{2-}$	0.01	82
Y6	7.5		0.04	219
Y7	7.5		0.06	975
Y8	7.5		0.09	799
Y9	9	$HAsO_4^{2-}$	0.01	105
Y10	9		0.04	548
Y11	9		0.06	789

[a] Speciation data have been taken from Pourbaix.[46]

TABLE 2: Atomic Positions in Unit Cell for Pure Gypsum[a]

atom		*X*	*Y*	*Z*	U_{iso} (Å^2)
Ca		0.5	0.0800(4)	0.25	0.0034(6)
	†	*0.5*	*0.07960(4)*	*0.25*	*0.0095(2)*
	‡	*0.5*	*0.0786(3)*	*0.25*	*0.0072*
S		0.0	0.0774(5)	0.75	0.0021(7)
	†	*0.0*	*0.07758(6)*	*0.75*	*0.0101(3)*
	‡	*0.0*	*0.0787(4)*	*0.75*	*0.0064*
O(1)		0.963(1)	0.1333(5)	0.550(1)	0.0104(9)
	†	*0.9631(2)*	*0.1317(1)*	*0.5478(2)*	*0.0088(4)*
	‡	*0.9616(5)*	*0.1326(1)*	*0.5512(4)*	*0.0149*
O(2)		0.759(1)	0.0217(5)	0.666(1)	0.0085(9)
	†	*0.7559(2)*	*0.0216(1)*	*0.6631(2)*	*0.0092(4)*
	‡	*0.7571(5)*	*0.0215(2)*	*0.6653(4)*	*0.0123*
O(3)		0.375(1)	0.1833(5)	0.457(1)	0.0133(9)
	†	*0.3796(3)*	*0.1822(1)*	*0.4592(2)*	*0.0151(4)*
	‡	*0.3784(6)*	*0.1826(2)*	*0.4564(5)*	*0.0222*
H(1)		0.247(3)	0.165(1)	0.509(3)	0.020(2)
	†	*0.250(3)*	*0.1536(7)*	*0.482(3)*	*0.085(6)*
	‡	*0.2504(6)*	*0.1615(2)*	*0.5009(6)*	*0.0446*
H(2)		0.399(3)	0.242(1)	0.491(3)	0.022(2)
	†	*0.409(4)*	*0.2412(5)*	*0.500(4)*	*0.085(6)*
	‡	*0.4023(7)*	*0.2435(2)*	*0.4900(6)*	*0.0389*

[a] Atomic positions from refs 29 (†) and 30 (‡) are given in italics for the sake of comparison.

Density functional theory (DFT) modeling of the pure and the arsenic-doped gypsum structures help us to understand the mechanisms of substitution of arsenate for sulfate and to elucidate how the charge is redistributed upon the substitution takes place. Finally, Mulliken population analyses allow quantifying the changes in the electrostatic interactions between ions for the different protonated/unprotonated species of arsenate.

2. Materials and Methods

2.1. Experimental Methods. Gypsum was precipitated from supersaturated solutions of calcium sulfate prepared by mixing directly into a reactor two equimolar aqueous solutions (0.5 M) of reagent-grade $CaC1_2$ and Na_2SO_4. The solutions were mixed under stirring to avoid the formation of local precipitates and the temperature was kept at 25 °C in a thermostatic water bath. Ten runs were conducted to produce samples at three different total arsenic concentrations and at three different pH values (4, 7.5 and 9), together with a pure gypsum reference sample (see Table 1 for sample description). Sodium arsenate dibasic heptahydrate ($Na_2HAsO_4 \cdot 7H_2O$) from Sigma Aldrich was used as the arsenate source in all the solutions. The pH values were recorded continually as a function of time during syntheses. Final solid arsenic concentrations in the solids were determined by Inductively Coupled Plasma Atomic Emission Spectrometry (ICP-AES) after dissolution in a 10 M HNO_3 solution (Table 1).

Powder samples were analyzed by neutron diffraction at the high flux powder diffractometer D20 at the Institut Laue-Langevin (ILL), and by X-ray diffraction at the ID11 Materials Science Beamline at the European Synchrotron Radiation Facility (ESRF), in Grenoble (France). Details of the experimental setup have been published elsewhere.[14] The neutron and X-ray diffraction data were analyzed by means of Rietveld analysis, using the FullProf software.[27] For neutron refinements a pseudo-Voigt function convoluted with an axial divergence asymmetry function was used to fit the shape of the peaks to correct for the large peak asymmetry at low diffraction angle. For the refinement of X-ray data a pseudo-Voigt function was used. Preferred orientation effects[28] affecting the intensity of the (010) reflection of the gypsum structure were considered in the refinements. The Rietveld refinement of the pure gypsum structure was carried out assuming a monoclinic unit cell with *C*2/*c* space group (no. 15) as starting model. The refined atomic parameters are given in Table 2 and compared with other published structures.[29,30] The refinements of the As-doped gypsum structures have been done by assuming the 4e Wyckoff sulfur position shared with the arsenic atom.

EXAFS spectra have been acquired on the BM8-GILDA beamline at the ESRF in Grenoble (France).[31] All the spectra have been measured at the arsenic K-edge (11867 eV) using a couple of Si (311) monochromator crystals. All the measurements have been performed at 77 K to reduce the thermal dumping of the signal.

The DFT optimizations of the arsenic-doped gypsum structure allow us to have a model for the local environment of the arsenic atom in the gypsum structure. We use this model as a starting point to calculate the amplitude and back-scattering functions with the FEFF8 code.[32] The coordination for each shell has been fixed to its ideal value, obtained from the DFT models, to reduce the correlation between free parameters in the minimization procedure, which were mainly the bond distances and the Debye−Waller factors. The latter take into account both dynamic (thermal induced) and static structural (if present) disorder. Other free parameters were the experimental energy shift and the EXAFS many-body loss factor (S_0^2). The data have been extracted using standard procedures.[33] The fits were performed using the MINUIT library from CERN.[34]

2.2. Theoretical Calculations. Geometrical optimizations of the gypsum unit cell and of 2 × 1 × 2, 2 × 1 × 3 and 3 × 1 × 3 supercells have been performed using the Vienna Ab-initio Simulation Package (VASP)[35] [$l \times m \times n$ representing a supercell of $l \times m \times n$ cells in directions *a*, *b* and *c*, respectively]. The calculations were performed at the Gamma point ($k = 0$), using projector augmented wave (PAW) pseudopotentials[36] with a plane wave cutoff of 209 eV and the Perdew−Burke−Ernzerhof (PBE) functional of the generalized gradient approximation (GGA). The residual external pressure (Pulay stress) at end of the relaxations was always equal to zero, so any extra compensation for the Pulay stress was required. The goal was to reproduce the expansion of the unit cell induced by the substitution of arsenic atoms within the gypsum structure. One unit cell of the structure of pure gypsum obtained from Rietveld refinements was used as starting point for all the models

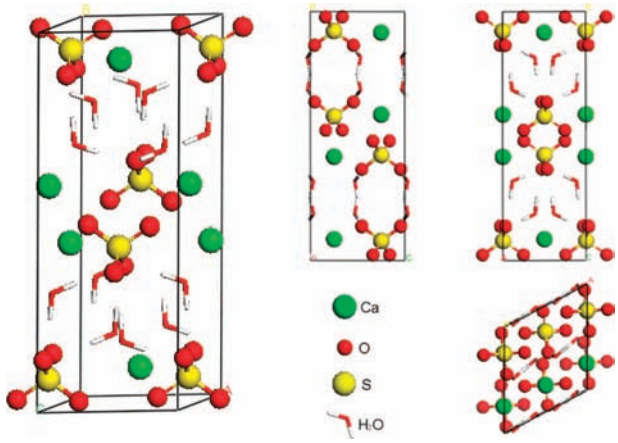

Figure 1. Left: view of the gypsum crystallographic unit cell. Right: orthogonal views of the gypsum unit cell with respect to the *A* crystallographic axis (up-left), *C* axis (up-right) and *B* axis (down-right).

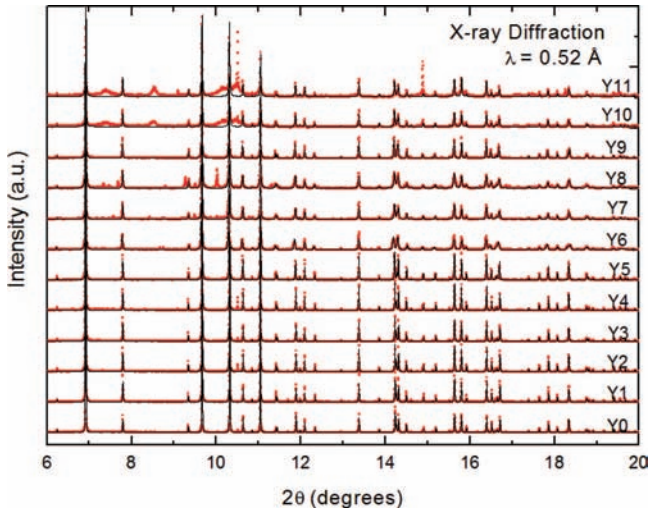

Figure 2. X-ray diffraction patterns. Points: experimental data. Lines: best fit.

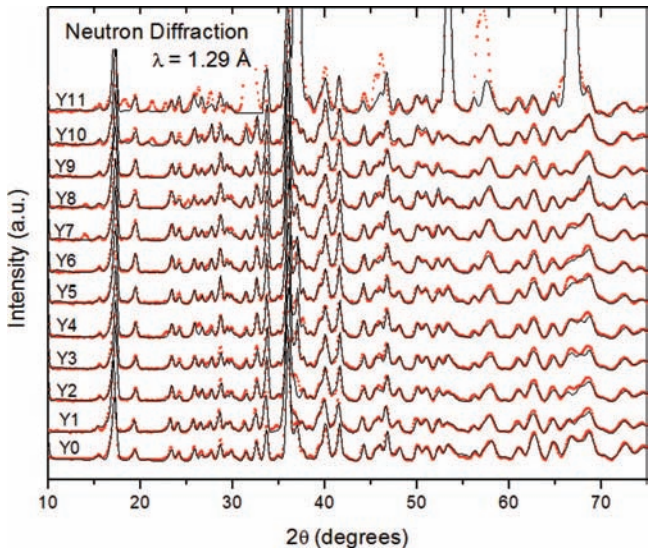

Figure 3. Neutron diffraction patterns. Points: experimental data. Lines: best fit.

(see Figure 1 for a model gypsum unit cell). The volume expansion induced by either the protonated $HAsO_4^{2-}$ or the unprotonated AsO_4^{3-} species was checked in single cells by

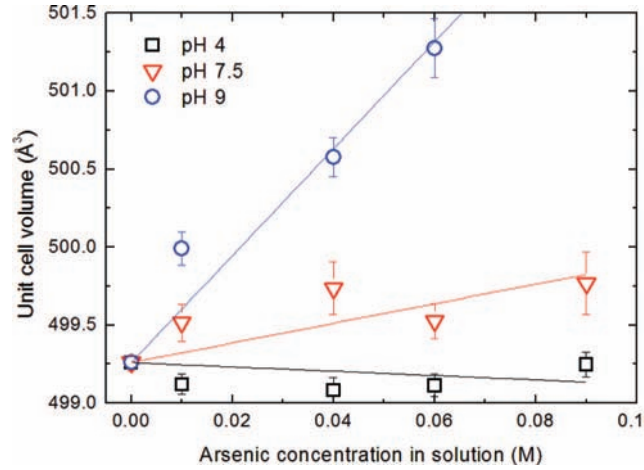

Figure 4. Unit cell volume for each of the samples. The common initial point for the three fit lines corresponds to the structure of pure gypsum.

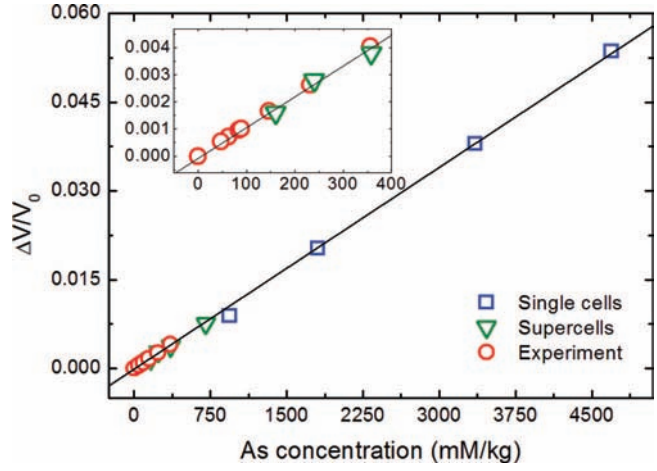

Figure 5. Simulated relative expansion of the unit cell volume of gypsum as a function of the arsenic concentration. The inset shows a detail of the interpolation of the experimental data using the simulated expansion.

replacing the four sulfate anions SO_4^{2-} until the replacement of all the sulfur atoms within the unit cell. The same kind of simulation was done with supercells of $2 \times 1 \times 2$, $2 \times 1 \times 3$ and $3 \times 1 \times 3$ to reach lower arsenic concentrations in the models. Relative volume variations are used to quantify the amount of arsenic in the gypsum cells. This allows us to avoid in the calculated unit cells of gypsum the effect of shrinkage due to the fact that the optimizations of the geometry are done at zero Kelvin.[37]

The replacement of sulfate groups by arsenate groups implies not only structural changes in the volume of the gypsum unit cell but also modifications in the electronic charge distribution, which affect the strength of the electrostatic interactions within the cells. Mulliken population analyses[38,39] (MPAs) have been performed to study these charge redistribution processes within the doped and pure gypsum structures. These calculations project into linear combinations of atomic orbitals (LCAOs) the charge density, thus obtaining values for atomic charges and bond populations.[39] For this reason it is generally acknowledged that population analyses give only semiquantitative information, as they are extremely sensitive to the atomic basis set used. However, relative variations of charge and bond populations of pure and doped models can be used to understand the underlying charge redistribution processes.[40–42]

TABLE 3: Unit Cell Parameters from Combined Refinement of Neutron and X-ray Data Together with Parameters Related to the Goodness of Refinements R-Bragg and χ^2 for Neutrons (RB_n, χ^2_n) and X-ray ($RB_{X\text{-}ray}$, $\chi^2_{X\text{-}ray}$)

pH	[As(V)] (M)	*a* (Å)	*b* (Å)	*c* (Å)	β (deg)	vol unit cell (Å^3)	RB_n	χ^2_n	$RB_{X\text{-}ray}$	$\chi^2_{X\text{-}ray}$
7.5	0.00	5.6929 (6)	15.245 (2)	6.5440 (4)	118.480 (4)	499.26 (2)	3.00	10.2	5.2	2.5
4	0.01	5.6923 (7)	15.245 (5)	6.5439 (4)	118.483 (1)	499.12 (1)	3.49	30	14.9	4.60
	0.04	5.6922 (1)	15.246 (4)	6.5429 (3)	118.480 (4)	499.08 (2)	7.45	60	12.3	4.03
	0.06	5.6923 (5)	15.246 (7)	6.5431 (8)	118.483 (5)	499.11 (2)	9.40	38.9	9.32	2.75
	0.09	5.6929 (2)	15.247 (1)	6.5436 (5)	118.479 (2)	499.24 (2)	9.21	46.6	16.9	4.23
7.5	0.01	5.6949 (5)	15.254 (9)	6.5406 (6)	118.441 (2)	499.61 (2)	4.54	27.6	11.4	3.48
	0.04	5.6956 (4)	15.258 (8)	6.5391 (7)	118.339 (6)	499.73 (6)	4.79	31.3	8.88	3.40
	0.06	5.6942 (3)	15.256 (6)	6.5389 (3)	118.432 (5)	499.52 (4)	4.30	32	9.88	3.83
	0.09	5.6955 (4)	15.259 (5)	6.5379 (7)	118.411 (4)	499.76 (7)	9.23	80.7	15.2	5.83
9	0.01	5.6973 (7)	15.264 (8)	6.5364 (2)	118.388 (3)	500.09 (2)	3.61	21	8.32	2.95
	0.04	5.7011 (8)	15.270 (8)	6.5329 (5)	118.427 (5)	500.57 (5)	7.18	31.9	28.4	3.73
	0.06	5.7010 (8)	15.272 (4)	6.5468 (9)	118.431 (7)	501.27 (8)	9.20	64.9	40.3	5.79

For all the MPAs calculations we used a commercial version of the plane wave pseudopotential code CASTEP., as implemented in Materials Studio (Accelrys Inc.). Mulliken charges and bond populations are calculated according to the formalism described by Segall et al.[40] MPAs have been performed on the cell models of the pure and doped gypsum structures that were optimized with VASP. Energy minimizations with fixed atomic positions have been performed using the VASP optimized structures prior to the calculation of the MPAs.

For the energy minimizations with CASTEP we used the PBE variation of the GGA.[44] We used ultrasoft pseudopotentials,[45] with a maximum cutoff energy of the plane waves of 340 eV. Another parameter that determines the quality of the calculations is the density of points with which the Brillouin zone is sampled; we used a parameter such that the distances between grid points are less than 0.15 Å^{-1}, comparable to the sampling used for the VASP calculations. Different values for the energy cutoff and different exchange functionals were checked in a first step to optimize the convergence of the calculations. The values of the Mulliken charges and bond populations have been shown to converge within the 5% of their value.

3. Results and Discussion

3.1. Volume Expansion and Local Environment of Arsenic. ***Diffraction Results.*** The neutron and X-ray diffraction patterns (Figures 2 and 3) show the existence of a solid phase with the structure of gypsum and of some other precipitates that cannot be identified within the Inorganic Crystal Structure Database (ICSD).[46] The Rietveld refinement of the atomic parameters of pure gypsum reveal a very well crystallized phase, as compared to other published structures (Table 2).

Only one out of ten of the arsenic-containing samples presents an important weight of other crystalline phase: the sample Y11 shows diffraction peaks of sodium chloride (NaCl) in its X-ray diffraction pattern (Figure 2). A poorly crystallized phase of an unknown precipitate is also found in this sample: the characteristic amorphous halo can be easily seen (Figure 2). These phases are not observed in the neutron diffraction patterns. This reflects the different sensitivity of the methods: X-rays are more sensitive to phases adsorbed on the surface and neutrons probe the bulk of the samples. In the neutron diffraction pattern of sample Y11 (Figure 3) the contribution from the vanadium sample holder can be distinguished. This is due to the fact that only a small volume of sample was available for the experiment. Therefore, a phase of vanadium was introduced in all the analyses of the neutron data. In the Rietveld refinements of the gypsum phase, the (4e) Wyckoff position corresponding to the sulfur atom has been shared with the arsenic atom, under the hypothesis that arsenate for sulfate substitution occurs. The lattice parameters of the phase of gypsum obtained from combined Rietveld refinements of neutron and X-ray data are shown in Table 3 together with the R-Bragg (RB) and χ^2 values of the fits.

A plot of this data set (Figure 4) gives a better understanding of the results. It shows an expansion of the unit cell proportional to the initial arsenic concentration in the solutions, and which slope is strongly dependent on the equilibrium pH value. The

TABLE 4: Bond Lengths and Debye−Waller Factors of the EXAFS Analyses of the Samples Y6, Y8 and Y11 and Bond Lengths of the Theoretical Model Obtained with the ab Initio Calculations

Y6			
path	*N*	*R* (Å)	σ^2 (Å^2)
As−O	4	1.68 ± 0.03	0.002 ± 0.003
As−Ca_1	1	3.16 ± 0.05	0.001 ± 0.004
As−Ca_2	1	3.31 ± 0.03	0.001 ± 0.004
As−Ca_3	1	3.71 ± 0.06	0.001 ± 0.004
Y8			
shell	*N*	*R* (Å)	σ^2 (Å^2)
As−O	4	1.67 ± 0.03	0.001 ± 0.003
As−Ca_1	1	3.14 ± 0.05	0.004 ± 0.005
As−Ca_2	1	3.22 ± 0.07	0.004 ± 0.005
As−Ca_3	1	3.70 ± 0.06	0.004 ± 0.005
Y11			
shell	*N*	*R* (Å)	σ^2 (Å^2)
As−O	4	1.68 ± 0.01	0.002 ± 0.001
As−Ca_1	1	3.18 ± 0.05	0.003 ± 0.004
As−Ca_2	1	3.30 ± 0.08	0.003 ± 0.004
As−Ca_3	1	3.70 ± 0.07	0.003 ± 0.004
Theoretical Model: $HAsO_4^{2-}$ in Gypsum			
shell	*N*	*R* (Å)	
As−O	4	(1.69) (1.69, 1.79)[a]	
As−Ca_1	1	3.10	
As−Ca_2	1	3.31	
As−Ca_3	1	3.70	
Theoretical Model: Pure Gypsum			
shell	*N*	*R* (Å)	
S−O	4	1.48	
S−$Ca_{1,2}$	2	3.12	
S−$Ca_{3,4}$	2	3.70	

[a] Path lengths of the first shell single scattering path for each of the two different ions: AsO_4^{3-} and $HAsO_4^{2-}$.

TABLE 5: Mulliken charges and Effective Ionic Valences for the Three Models of Pure and Doped Gypsum[a]

material	ion	atom	Mulliken charge	effective ionic valence
gypsum	SO_4^{2-}		−1.38	0.62
		S	2.38	
		$O_{1,2}$	−0.95	
		$O_{3,4}$	−0.93	
	$Ca_{1,2,3,4}^{2+}$		1.42	0.58
	spilling parameter $s_1 = 1.3 \times 10^{-2}$			
$HAsO_4$ doped gypsum	$HAsO_4^{2-}$		−1.37	0.63
		As	2.25	
		$O_{1,2}$	−0.90	
		O_3	−0.88	
		O_4	−0.94	
		H	0.44	
	$Ca_{1,2}^{2+}$		1.37	0.63
	Ca_3^{2+}		1.39	0.61
	Ca_4^{2+}		1.41	0.59
	spilling parameter $s_2 = 1.2 \times 10^{-2}$			
AsO_4 doped gypsum	AsO_4^{3-}		−1.29	1.71
		As	2.24	
		$O_{1,2}$	−0.89	
		O_3	−0.87	
		O_4	−0.88	
	$Ca_{1,2}^{2+}$		1.30	0.70
	$Ca_{3,4}^{2+}$		1.37	0.63
	spilling parameter $s_3 = 1.1 \times 10^{-2}$			

[a] The spilling parameter for each of the calculations is also presented. The labels of the atoms are explained on Figure 7. Both the Mulliken charges and the effective ionic valence values are given in e^-.

biggest expansion is found in samples synthesized at pH 9, indicating a preference of the unit cell of gypsum to host protonated arsenate ions $HAsO_4^{2-}$ ($pK_2 = 7.08$, $pK_3 = 11.5$).[47] This result is in agreement with the results expected under the hypothesis of a charge balanced replacement. The charge developed by the arsenate species at different pH values is shown in Table 1.[47]

Modeling Results. Simulations help us to understand the volume expansion. Gypsum cells with both the protonated and unprotonated arsenates were simulated separately. Models of four single cells with one to four arsenate ions each (giving arsenic concentrations of 940, 1809, 3357 and 4696 mM/kg) and four supercells were simulated: two $2 \times 1 \times 2$ supercells with one (358 mM/kg) and two (705 mM/kg) As atoms, and supercells of $2 \times 1 \times 3$ (240 mM/kg) and $3 \times 1 \times 3$ (160 mM/kg) with one arsenic atom each. Same size supercells of pure gypsum have been simulated as well. The obtained cell parameters differ by less than 3% from the experimental ones.

The simulations show an expansion of the unit cell volume proportional to the number of sulfate ions that have been substituted by arsenates, following a linear Vegard's law behavior (Figure 5). It is important to note that the same volume expansion is found for substitutions of protonated and unprotonated arsenate for sulfates.

The crystalline structure of gypsum has (010) planes where Ca^{2+} and SO_4^{2-} ions interact through ionic bonding. These planes are held together by H-bonds through water molecules that sit in between them. The S−O bond distance within a sulfate group in the gypsum structure is 1.47 Å.[48] The As−O bond length is roughly 1.69 Å,[49] increasing up to 1.79 Å when an H atom is bound to an O in the protonated species. Due to the higher volume of the arsenate ion with respect to the sulfate, the degeneracy of the two X−Ca interatomic distances, that is, 2-fold in the pure gypsum structure (X = S), is broken, giving four different X−Ca distances in the arsenic-doped gypsum (X = As), as indicated in Table 4. This induces an increase of the lattice parameters *a* and *c*. The interplanar distance between hydrogen-bonded planes expands as well, increasing the lattice parameter *b*. These changes in the structure result in a volume expansion of the crystal lattice of arsenic-doped gypsum, as indicated in Figure 5.

The models allow us to extrapolate the arsenic concentration in the bulk of the samples by comparing the relative volume variations between the experimental and simulated data. The experimental values of the volume expansion have been interpolated in the linear fit that describes the model expansion of the volume (inset Figure 5), giving maximum values for the concentration of arsenic incorporated in the crystallographic structure of gypsum. These concentrations (Table 7) are smaller than the total concentration of arsenic found in the samples (adsorbed and substituted).

EXAFS Results. EXAFS is used to study the immediate atomic environment around a selected absorber atom (up to no more than 10 Å) without requiring long-range order of the lattice (a requirement for diffraction techniques). For these reasons, EXAFS is a genuine local and selective probe which can provide complementary information on the lattice structure with respect to diffraction techniques.

The *k*-weighted EXAFS oscillations and the fit curves for the samples Y6, Y8, and Y11 are shown in Figure 6. The obtained absorber-backscatterer distances are shown in Table 5 and show a good agreement with the modeled structure. The three samples show little difference in the local atomic environment: the first shell is formed by oxygen atoms in tetrahedral coordination (4-fold degenerated) at a distance of $d_{As-O} = 1.69$ Å. One of the four As−O distances is 1.79 Å in the theoretical model of the $HAsO_4^{2-}$ ion, which is impossible to distinguish due to the limited resolution of our experimental conditions. The second shell signal originates from the As−Ca bonds which are split in three singly degenerate distances: $d_{AsCa1} = 3.15$ Å, $d_{As-Ca2} = 3.31$ Å and $d_{As-Ca3} = 3.70$ Å. Contributions from higher coordination shells fall under the detectable threshold. The results are in good agreement with the scenario of replacement of $HAsO_4^{2-}$ for SO_4^{2-}. The As−Ca distances calculated with the DFT modeling agree with experimental values within error bars (Table 5).

3.2. Charge Balance. Charge balance is a strict requirement for any equilibrated substitution that may occur in ion exchange processes. However, the nature of the balancing mechanism can be local or global. Recently, some authors have demonstrated experimentally that the arsenite molecule (AsO_3^{3-}) replaces carbonate molecules in the calcite structure, which results in a nonbalanced local charge.[20] In the same way, other authors hypothesize that the charge balance of uranyl ions incorporated in calcite through a nonlocal mechanism by which Na^+ cations would be compensating the charge.[22] In the case of gypsum, the existence of a "water interlayer" in the structure (see Figure 1) provides mechanisms for charge balancing, if sulfate is being substituted by the unprotonated AsO_4^{3-} species: formation of H_3O^+ molecules is a valid hypothesis that would make the unprotonated arsenate by sulfate substitution hence possible. Other possibilities could include the existence of defects or interstitials, as the inclusion of extra Ca^{2+} cations in the ionic layer. However, our EXAFS data fits very well with the calculated model for the inclusion of the protonated $HAsO_4^{2-}$, reproducing accurately the distances found in the simulated models. Thus, the existence of a local charge balance mechanism is corroborated experimentally with a local probe (EXAFS). In

TABLE 6: Bond Lengths (Å) and Bond Populations (e^- $Å^{-3}$)[a]

SO_4^{2-}			$HAsO_4^{2-}$			AsO_4^{2-}		
atoms	bond length	bond population	atoms	bond length	bond population	atoms	bond length	bond population
Ca−S	3.12	−0.20	Ca−As	3.08	−0.35	Ca−As	3.15	−0.73
Ca1−O1	2.53	0.06	Ca1−O1	2.47	0.08	Ca1−O1	2.56	0.06
Ca1−O3	2.52	0.06	Ca1−O3	2.60	0.03	Ca1−O3	2.42	0.10
Ca2−O2	2.53	0.06	Ca2−O2	2.56	0.06	Ca2−O2	2.56	0.06
Ca2−O4	2.52	0.06	Ca2−O4	2.43	0.08	Ca2−O4	2.42	0.10
Ca3−O3	2.35	0.09	Ca3−O3	2.41	0.05	Ca4−O3	2.28	0.12
Ca4−O4	2.35	0.09	Ca4−O4	2.56	0.06	Ca3−O4	2.28	0.12
⟨Ca−O⟩	2.47	0.07	⟨Ca−O⟩	2.45	0.07	⟨Ca−O⟩	2.42	0.10

[a] A negative number in the bond population means the character of the bond is antibonding. ⟨x⟩ stands for the mean value. The labels of the atoms are explained on Figure 7.

TABLE 7: Concentration of Arsenic Incorporated into the Bulk of Gypsum[a]

initial [As] in solution (M)	pH 4 [As] (mM/kg)	pH 7.5 [As] (mM/kg)	pH 9 [As] (mM/kg)
0.01	0	62	145
0.04	0	84	232
0.06	0	46	355
0.09	0	89	

[a] The values have been obtained by interpolating the experimental volume expansion data in the theoretical volume expansion curves.

this context, the electrostatic effects of a local substitution mechanism ($HAsO_4^{2-}$) and of a nonlocal substitution mechanism (AsO_4^{3-}) will be shown.

Under oxidizing conditions and at pH higher than p$K_2 = 11.5$, unprotonated arsenate (AsO_4^{3-}) becomes the aqueous arsenic dominant species. Unprotonated arsenate is an ion with C_2 tetrahedral symmetry very similar to sulfate ions (SO_4^{2-}), with T_d symmetry. From the point of view of symmetry, the very similar geometry of both ions would suggest that the replacement is more likely under very alkaline conditions (i.e., at pH higher than 11), where AsO_4^{3-} is thermodynamically the more stable species. The fact that the same volume expansion is found for both AsO_4^{3-} and $HAsO_4^{2-}$ implies that any assumption of which species is responsible for the volume expansion cannot be made a priori. In the protonated $HAsO_4^{2-}$, species of lower symmetry than AsO_4^{3-}, the As−O bond length is increased for the O atom bonded to the H atom.

To evaluate the strength of electrostatic interactions within the gypsum structure and their changes when a sulfate ion is substituted by an arsenate, we have performed MPAs in the pure and doped structures of gypsum. As stated above, the gypsum structure is formed by planes of ionic bonded Ca^{2+} and SO_4^{2-} ion pairs; these planes are hold together by H-bonds through water molecules located in between the planes (view Figure 1). When an arsenate ion substitutes a sulfate, the degree of ionicity of both the Ca^{2+} and the anions is changed, and the aim of these analyses is to quantify these changes.

This kind of analysis gives values for the charge by integrating into LCAOs the charge density distribution which results from the energy optimization of the DFT calculation. Different values for the charges are assigned to each atom, as well as values for the bond populations and its bonding or antibonding character.

The ionicities of the Ca^{2+} cations and of the AsO_4^{3-}, $HAsO_4^{2-}$ and SO_4^{2-} ions in the structure of gypsum have been evaluated by calculating their effective ionic valence, which has been defined as the difference between the formal ionic charge and the Mulliken charge of the ion species in the crystal.[41] In the case of an ideal ionic bond the effective ionic valence has a null value, whereas values greater than zero indicate increasing levels of covalency. We have evaluated the Mulliken charges for all the atoms and the bond populations for the bonds with lengths up to 3.5 Å in all the three different models: pure gypsum, $HAsO_4^{2-}$ doped gypsum and AsO_4^{3-} doped gypsum. The effective ionic charges have been calculated considering a formal valence of +2 for the Ca^{2+}, SO_4^{2-} and $HAsO_4^{2-}$ ions (without considering the charge of the H atom in the latter), and a formal charge of +3 for the AsO_4^{3-} ion.

Results are shown on Tables 5 and 6, together with the spilling parameter of each of the calculations. This parameter indicates the percentage of valence charge that has been missed in the projection. A low spilling parameter indicates a good representation of the electronic bands using the LCAO basis set. The effective ionic valence for the four Ca^{2+} cations (see Figure 7) in pure gypsum is 0.58 e^-. The $HAsO_4^{2-}$ doped gypsum has values for the Ca^{2+} effective ionic valence that range from 0.59 e^- to 0.63 e^-. The Ca^{2+} cations in the AsO_4^{3-} doped gypsum have values of 0.70 e^- and 0.63 e^-.

The degree of covalency can also be evaluated through the bond populations. Results are shown in Table 6, and can be summarized in two points:

(1) The values for the Ca−O bond populations in the AsO_4^{3-} doped gypsum are higher than in the other two structures. The Ca−O bond population in the pure gypsum has a mean value of 0.07 e^-, exactly equal to that of the $HAsO_4^{2-}$ doped gypsum, and the mean value in the AsO_4^{3-} doped gypsum is 0.095 e^-.

(2) The bond population of the Ca−S or Ca−As bonds are −0.20 e^- in the pure gypsum (negative value meaning that the antibonding orbital is populated), −0.35 e^- in the $HAsO_4^{2-}$ doped gypsum and −0.73 e^- in the AsO_4^{3-} doped gypsum.

These results can be interpreted in terms of a redistribution of the extra valence electron introduced with the AsO_4^{3-} ion over its neighbors. They reflect an increase of the covalency in the Ca^{2+} - AsO_4^{3-} interaction. In the $HAsO_4^{2-}$ ion the H atom acts as a charge "reservoir" for this electron, thus not allowing the extra electron to spread over its neighbors. This results in a higher degree of ionicity in the Ca^{2+} - $HAsO_4^{2-}$ interaction, similar to the Ca^{2+} - SO_4^{2-} ionicity in pure gypsum structure.

The mean Ca−O, Ca−As and Ca−S interatomic distances are presented in Table 6. The higher volume of the arsenate ion with respect to the sulfate is reflected in the shortening of these distances. In principle, a shorter distance would give rise to an increase of the covalency, as the overlap between the orbitals would be higher. However, the results of these analyses show that this is not the case for the $HAsO_4^{2-}$ ion. The effective ionic valence of its atoms and the bond population values are very similar to the values of the pure gypsum structure. Hence, low incorporation of AsO_4^{3-} molecules can be expected in the

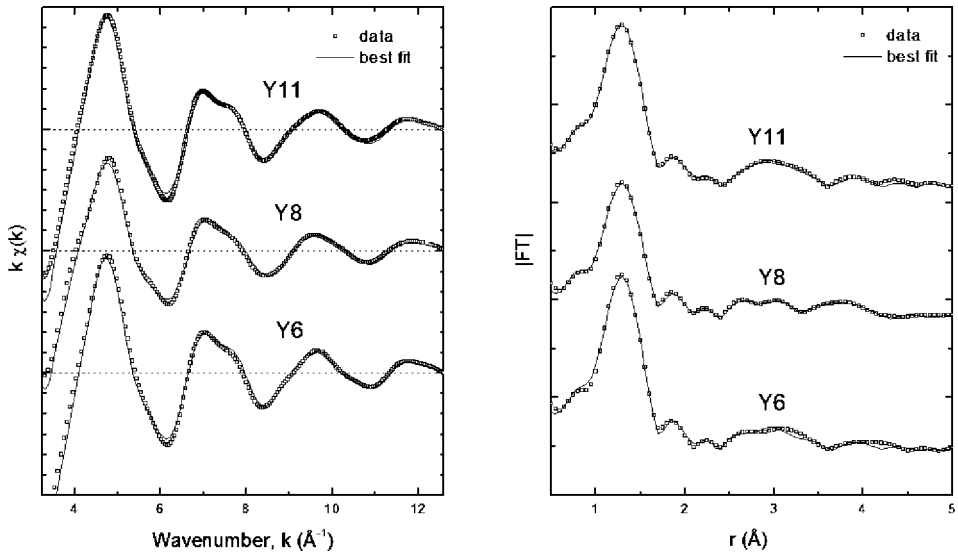

Figure 6. EXAFS signals and fit curves for the Y6, Y8, and Y11 samples in the *k* space (3.5−12 Å^{-1}) and their respective Fourier tranforms (distances not corrected for phase shifts).

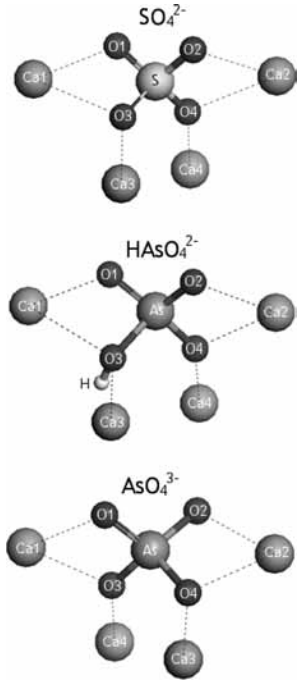

Figure 7. Atomistic models of the SO_4^{2-}, $HAsO_4^{2-}$ and AsO_4^{3-} and their closer Ca shells within the structure of gypsum. The dotted lines indicate the shorter Ca−O distances.

absence of any nonlocal mechanism of charge balancing (interstitials, ...).

4. Conclusions

The ability of arsenate to isomorphically substitute for sulfate in the gypsum structure is demonstrated in the present study by measuring the volume expansion of the unit cell with neutron and X-ray diffraction techniques. This volume expansion has been found to increase with the equilibrium pH value, up to pH 9. This is in agreement with the evolution of the concentration of $HAsO_4^{2-}$ ions in solution. At pH 4 only a very low percentage of the arsenates are protonated, $H_2AsO_4^-$ being the dominant species. As pH increases, $HAsO_4^{2-}$ becomes the dominant species, thus giving rise to a higher rate of isomorphic substitution within gypsum.

Simulations allow us to reproduce the expansion of the volume of the unit cell as arsenic is increasingly substituted for sulfur. A similar expansion is found for both the $HAsO_4^{2-}$ and the AsO_4^{3-} doped gypsum structures, indicating that the extra proton introduced in $HAsO_4^{2-}$ does not have any influence on the volume of the ion itself. However, MPAs show the influence of the H atom as an electron reservoir that makes the substitution of arsenic (pentavalent) for sulfur (tetravalent) possible. The values of the theoretical expansion of the volume help us to make an estimation of the total amount of arsenic that can be hosted into the bulk of gypsum in ideal conditions (Table 7).

The local structure of the arsenic atom in the bulk of gypsum has been probed by XAS. Two different shells can be distinguished: one formed by four oxygen atoms, constituting the arsenate ion, and a second shell formed by calcium atoms placed at three different distances. These distances coincide within the experimental error with the distances of the DFT optimized structure of $HAsO_4^{2-}$ doped gypsum.

The MPAs have helped us to understand how the charge is redistributed upon substitution, and to elucidate what would happen if this substitution took place at a higher pH value, where the AsO_4^{3-} species is the most stable. The models show that the protonated arsenate species is introduced in the gypsum structure conserving the degree of ionicity of the ion pairs $Ca^{2+}-SO_4^{2-}$. The extra proton acts as a charge reservoir for the extra electron introduced within the $HAsO_4^{2-}$ ion. This is not the case for the $Ca^{2+}-AsO_4^{3-}$ interactions, where the ionicity is reduced, making the substitution process less likely. Recently, some experimental results of EPR measurements on another ionic mineral, namely natural calcite[22] have demonstrated the ability of calcite to host As atoms in its bulk through a similar substitution mechanism (arsenite AsO_3^{3-} for carbonate CO_3^{2-}), in which the charge is not balanced, at least at a local (few Angstroms) scale. Even though direct observation of the local structure of the arsenic atom in calcite has to our knowledge not yet been published, we think that a modeling approach could help to understand the effect of this mechanism of substitution on the electrostatic interactions within the calcite structure.

Our results support the hypothesis of arsenic immobilization by incorporation into the bulk of gypsum. When a hazardous

ion like arsenate is incorporated into the bulk of a mineral, it can be considered immobilized, reducing its mobility and the potential risk of environmental contamination. Quantifying the exact concentration of arsenic that can be hosted into the gypsum structure can help to improve the knowledge on the long-term stability of contaminated sludges and has important consequences for site remediation actions.

Acknowledgment. We thank Dr. Gavin Vaughan and Dr. Javier Campo for their assistance in the diffraction experiments, the Italian CRG GILDA and ID11 (Experiment ME-171) beamlines at the ESRF and the ILL (Experiment 5-25-57) for the allocation of the beamtime. Contributions from three anonymous reviewers are kindly acknowledged. This work was partially supported by the Action ECOS-SUDA02U01 and EC2CO CNRS program.

References and Notes

(1) Nriagu, J. O. *Arsenic in the Environment. Part I: Cycling and Characterization*; Wiley Series in Advances in Environmental Science and Technology; Wiley: New York, 1994; Vol. 26.

(2) Smedley, P. L.; Kinniburgh, D. G. *Appl. Geochem.* **2002**, *12*, 517.

(3) Juillot, F.; Ildefonse, P. H.; Morin, G.; Calas, G.; De Kersabiec, A. M.; Benedetti, M. *Appl. Geochem.* **1999**, *14*, 1031.

(4) Charlet, L.; Ansari, A. A.; Lespagnol, G.; Musso, M. *Sci. Total Environ.* **2001**, *277*, 133.

(5) Sadiq, M. *Wat., Air Soil Pollut.* **1995**, *93*, 117.

(6) Morin, G.; Juillot, F.; Casiot, C.; Bruneel, O.; Personne, J.-C.; Elbaz-Poulichet, F.; Leblanc, M.; Ildefonse, P.; Calas, G *Environ. Sci. Technol.* **2003**, *37*, 1705.

(7) Tournassat, C.; Charlet, L.; Bosbach, D.; Manceau, A. *Environ. Sci. Technol.* **2002**, *36*, 493.

(8) Román-Ross, G.; Charlet, L.; Cuello, G. J.; Tisserand, D *J. Phys. IV* **2003**, *107*, 1153.

(9) Fernández-Martínez, A.; Román-Ross; G.; Cuello, G. J.; Turrillas, X.; Charlet, L.; Johnson, M. R.; Bardelli, F. *Phys. B* **2006**, *935*, 385–386.

(10) Román-Ross, G.; Cuello, G. J.; Turrillas, X.; Fernández-Martínez, A.; Charlet, L. *Chem. Geol.* **2006**, *233*, 328.

(11) Sobolev, O.; Cuello, G. J.; Román-Ross, G.; Skipper, N. T.; Charlet, L. *J. Phys. Chem. A* **2007**, *111*, 5123.

(12) Pitteloud, C.; Powell, D. H.; González, M. A.; Cuello, G. J. *Colloids Surf. A* **2003**, *217*, 129.

(13) Stumpf, T.; Fernandes, M. M.; Walther, C.; Dardenne, K.; Fanghanel, T. *J. Colloid Interface Sci.* **2006**, *302*, 240.

(14) Fernandes, M. M.; Stumpf, T.; Rabung, T.; Bosbach, D.; Bauer, A.; Fanghanel, T *Geochim. Cosmochim. Acta* **2004**, *68*, A85.

(15) Dossier 2005 Argile. Référentiel du comportement des radionucléides et des toxiques chimiques d'un stockage dans le Callovo-Oxfordien jusqu'à l'homme. ANDRA, 2005.

(16) Cheng, L. W.; Fenter, P.; Sturchio, N. C.; Zhong, Z.; Bedzyk, M. J *Geochim. Cosmochim. Acta* **1999**, *63*, 3153.

(17) Lamble, G. M.; Reeder, R. J.; Northrup, P. A *J. Phys. IV* **1997**, *7*, 793.

(18) Cheng, L.; Sturchio, N. C.; Woicik, J. C.; Kemner, K. M.; Lyman, P. F.; Bedzyk, M. J. *Surf. Sci.* **1998**, *415*, 976.

(19) Cheng, L.; Sturchio, N. C.; Bedzyk, M. J. *Phys. Rev. B* **2000**, *61*, 4877.

(20) Di Benedetto, F.; Costagliola, P.; Benvenuti, M.; Lattanzi, P.; Romanelli, M.; Tanelli, G. *Earth Planet. Sci. Lett.* **2006**, *246*, 458.

(21) Sturchio, N. C.; Antonio, M. R.; Soderholm, L.; Sutton, S. R.; Brannon, J. C. *Science* **1998**, *281*, 971.

(22) Kelly, D. D.; Newville, M. G.; Cheng, L.; Kemner, K. M.; Sutton, S. R.; Fenter, P.; Sturchio, N. C.; Spötl, C. *Environ. Sci. Technol.* **2003**, *37*, 1284.

(23) *Active and Semi-Passive Lime Treatment of Acid Mine Drainage*; United States Environmental Protection Agency: Washington, DC, May 2006.

(24) Gominšek, T.; Lubej, A.; Pohar, C. *J. Chem. Technol. Biotechnol.* **2005**, 80–939.

(25) Paktunc, D.; Dutrizac, J. E. *Can. Miner.* **2003**, *41*, 905.

(26) Fernández-González, A.; Andara, A.; Alía, J. M.; Prieto, M. *Chem. Geol.* **2006**, *225*, 256.

(27) Rodríguez-Carvajal, J. *Physica B* **1993**, *192*, 55.

(28) Grattan-Bellew, P. E. *Am. Mineral.* **1975**, *60*, 1127.

(29) De la Torre, A. G.; López-Olmo, M. G.; Álvarez-Rúa, C.; García-Granda, S.; Aranda, M. A. G. *Power Diff.* **2004**, *19*, 240.

(30) Schofield, P. F.; Knight, K. S.; Stretton, I. C. *Am. Mineral.* **1996**, *81*, 847.

(31) Pascarelli, S.; Boscherini, F.; D'Acapito, F.; Hrdy, J.; Meneghini, C.; Mobilio, S. *J. Synchrotron Radiat.* **1996**, *3*, 147.

(32) Ankudinov, A. I.; Ravel, B.; Rehr, J. J.; Conradson, S. D. *Phys. Rev. B* **1998**, *58*, 7565.

(33) Lee, P. A.; Citrin, P. H.; Eisenberger, P.; Kincaid, B. M. *Rev. Mod. Phys.* **1981**, *53*, 769.

(34) James, F. *CERN Program Library* **1994**, 506.

(35) Kresse, G.; Hafner, J. *Phys. Rev. B* **1993**, *47*, 558. (a) Kresse, G.; Hafner, J. *Phys. Rev. B* **1994**, *49*, 14251. (b) Kresse, G.; Furthmüller, J. *Comput. Mater. Sci.* **1996**, 6–15. (c) Kresse, G.; Furthmüller, J. *Phys. Rev. B* **1996**, *54*, 11169.

(36) Kresse, G.; Joubert, D. *Phys. Rev. B* **1999**, *59*, 1758.

(37) Mihalkovic, M.; Widom, M. *Phys. Rev. B* **2004**, *70*, 144107.

(38) Mulliken, R. S. *J. Chem. Phys.* **1955**, *23*, 1833.

(39) Sánchez-Portal, D.; Artacho, E.; Soler, J. M. *Solid State Commun.* **1995**, *95*, 685.

(40) Segall, M. D.; Pickard, C. J.; Shah, R.; Payne, M. C. *Mol. Phys.* **1996**, *89*, 571.

(41) Segall, M. D.; Shah, R.; Pickard, C. J.; Payne, M. C. *Phys. Rev. B* **1996**, *54*, 16317.

(42) Winkler, B.; Pickard, C. J.; Segall, M. D.; Milman, V. *Phys. Rev. B* **2001**, *63*, 214103.

(43) Clark, S. J.; Segall, M. D.; Pickard, C. J.; Hasnip, P. J.; Probert, M. J.; Refson, K.; Payne, M. C. *Z. Kristallogr.* **2005**, *220*, 567.

(44) Perdew, J. P.; Burke, K.; Ernzerhof, M *Phys. Rev. Lett.* **1996**, *77*, 3865. (a) Perdew, J. P.; Burke, K.; Ernzerhof, M. *Phys. Rev. Lett.* **1997**, *78*, 1396.

(45) Kresse, G.; Hafner, J. *J. Phys.: Condens. Matter* **1994**, *6*, 8245.

(46) Inorganic Crystal Structure Database (ICSD) [http://icsd.ill.fr/icsd/].

(47) Pourbaix, M. *Atlas of Electrochemical Equilibria in Aqueous Solutions*; Pergamon Press: London, 1974.

(48) Kolitsch, U. *Acta Crystallogr., Sect. C* **2004**, *60*, i94–i96.

(49) Loureiro, S. M.; Radaelli, P. G.; Antipoc, E. V.; Capponi, J. J.; Souletie, B.; Brunner, M.; Marezio, M. *J. Solid State Chem.* **1996**, *121*, 66.

JP076067R